Low-spin signature inversion in the $\pi h_{9/2} \otimes \nu i_{13/2}$ oblate band of ^{190}Tl

C. Y. Xie,[1,2] X. H. Zhou,[1,2,*] Y. H. Zhang,[1] Y. X. Guo,[1] X. G. Lei,[1] Y. Zheng,[1] M. L. Liu,[1] L. T. Song,[1] H. L. Wang,[1] W. T. Guo,[1] H. P. Yu,[1] L. H. Zhu,[3] X. G. Wu,[3] and F. R. Xu[4]

[1]*Institute of Modern Physics, Chinese Academy of Sciences, Lanzhou 730000, China*

[2]*Graduate School of the Chinese Academy of Sciences, Beijing 100049, China*

[3]*China Institute of Atomic Energy, Beijing 102413, China*

[4]*Department of Technical Physics and MOE Key Laboratory, Peking University, Beijing 100871, China*

(Received 24 November 2004; published 12 October 2005)

High-spin states in ^{190}Tl have been studied experimentally by using the ^{160}Gd(^{35}Cl,5n) fusion-evaporation reaction at beam energies of 167 and 175 MeV. A rotational band built on the $\pi h_{9/2} \otimes \nu i_{13/2}$ configuration with oblate deformation has been established for ^{190}Tl. Spin values are assigned by adopting the results from α-γ decay work for ^{194}Bi found in the literature. With the configuration and spin-parity assignments, the low-spin signature inversion has been revealed for the $\pi h_{9/2} \otimes \nu i_{13/2}$ oblate band in ^{190}Tl. It is the first experimental observation of low-spin signature inversion for a band associated with the oblate $\pi h_{9/2} \otimes \nu i_{13/2}$ configuration. The low-spin signature inversion for the oblate $\pi h_{9/2} \otimes \nu i_{13/2}$ band can be interpreted by the two-quasiparticle-plus-rotor model including a J-dependent p-n residual interaction.

DOI: 10.1103/PhysRevC.72.044302 PACS number(s): 21.10.Re, 23.20.Lv, 27.80.+w

I. INTRODUCTION

It is generally suitable to classify a nuclear rotational band by the quantum number of signature α, which is related to the invariance of the intrinsic Hamiltonian of an axially deformed nucleus with respect to 180° rotation around a principle axis [1–3]. For a nuclear system with an odd particle number, the signature defined by $\alpha_f = 1/2(-1)^{j-1/2}$ (favored) is usually lower in energy with respect to the signature $\alpha_{\rm uf} = 1/2(-1)^{j+1/2}$ (unfavored) [1], where the angular momentum of the subshell associated with the odd particle is expressed by j. The signature splitting Δe is defined as the difference in energies at a given rotational frequency for the pair of signature partners. The signature α is an additive quantum quantity; therefore in odd-odd deformed nuclei the expected favored signature (α^f_{p-n}) of a two-quasiparticle band should result from the coupling between the favored signatures of both proton (α^f_p) and neutron (α^f_n) orbitals, while the unfavored signature ($\alpha^{\rm uf}_{p-n}$) corresponds to either $\alpha^f_p + \alpha^{\rm uf}_n$ or $\alpha^{\rm uf}_p + \alpha^f_n$ [2]. Signature inversion occurs if the expected favored signature branch of a rotational band lies higher in energy than the unfavored signature branch. Low-spin signature inversion has been systematically observed in deformed odd-odd nuclei throughout the chart of nuclides (see Refs. [2,4–10], and references therein), related to the high-j $\pi g_{9/2} \otimes \nu g_{9/2}$, $\pi h_{11/2} \otimes \nu h_{11/2}$, $\pi h_{11/2} \otimes \nu i_{13/2}$, $\pi h_{9/2} \otimes \nu i_{13/2}$, and $\pi i_{13/2} \otimes \nu i_{13/2}$ configurations. Great theoretical efforts have been devoted to the understanding of low-spin signature inversion in deformed odd-odd nuclei. Nuclear triaxiality and proton-neutron residual interaction have been proposed as possible reasons for the inversion phenomenon [2,6,7,11–14]. Furthermore, theoretical studies have suggested that the occurrence of signature inversion is associated closely with the positions of the Fermi surfaces of nucleons [2,15] and the configurations of states [14]. Therefore the observation of signature inversion bands in new mass regions and with new configurations is very important for a deeper understanding of the low-spin signature inversion phenomenon and for examining theoretical models with different physical pictures.

In the past few years experimental studies on doubly odd nuclei, located on the outer edge of the deformed rare-earth region, showed that the signature inversion phenomenon occurs generally in the prolate $\pi h_{9/2} \otimes \nu i_{13/2}$ bands in nuclei with $Z \leqslant 79$ (see Refs. [4,6,7,16] and references therein). In these bands, the $\alpha^f_{p-n} = \alpha^f_p + \alpha^f_n = 1/2 + 1/2 = 1$ favored signature branch lies higher in energy than the $\alpha^{\rm uf}_{p-n} = \alpha^f_p + \alpha^{\rm uf}_n = 1/2 - 1/2 = 0$ unfavored signature branch at low and medium spins, and the signature splitting reverts to the normal ordering at higher-spin states [4,6,7,16]. However, the signature inversion associated with the oblate $\pi h_{9/2} \otimes \nu i_{13/2}$ configuration has not been definitely established so far owing to experimental difficulties. Considering the general occurrence of signature inversion in rotational bands built on high-j orbitals both for protons and neutrons in doubly odd nuclei, it is natural to assume that the oblate $\pi h_{9/2} \otimes \nu i_{13/2}$ bands might also exhibit the phenomenon of low-spin signature inversion. The neutron-deficient doubly odd Tl nuclei, in which the rotational band built on the oblate $\pi h_{9/2} \otimes \nu i_{13/2}$ configuration dominates the yrast states [17–21], should provide the best candidate to search for signature inversion. Although bands based on the $\pi h_{9/2} \otimes \nu i_{13/2}$ oblate configuration were observed in doubly odd $^{192-200}$Tl [17–21], their spins could not be assigned unambiguously. As a consequence of this, interpretation of the distinctive energy staggering between the odd and the even spin member in these bands has remained uncertain, and two completely different models were proposed to interpret the staggering [21,22]. Fortunately, the α-γ correlation measurements in the α-decay studies of odd-odd

*Electronic address: zxh@impcas.ac.cn

Bi isotopes provided detailed information on the low-lying normal and intruder excited states in the daughter $^{184-192}$Tl nuclei [23,24]. This could help us unambiguously determine the spin and parity values of the oblate $\pi h_{9/2} \otimes \nu i_{13/2}$ bands in certain odd-odd Tl nuclei.

In this paper we report the first observation of low-spin signature inversion in the oblate $\pi h_{9/2} \otimes \nu i_{13/2}$ band of ^{190}Tl. Prior to this work, information on the low-lying excited levels in ^{190}Tl was obtained through the studies of the β^+/EC decay of ^{190}Pb [25] and the α decay of ^{194}Bi [23,24]. An early in-beam work [26] identified a long-lived isomer with an oblate configuration of $\pi h_{9/2} \otimes \nu i_{13/2}$ in ^{190}Tl, and three γ lines were suggested to be above the isomer.

II. EXPERIMENTS AND RESULTS

The excited states in ^{190}Tl were populated via the ^{160}Gd (^{35}Cl, $5n$)^{190}Tl reaction. The ^{35}Cl beam was provided by the HI-13 tandem accelerator of the China Institute of Atomic Energy (CIAE). The target was an isotopically enriched ^{160}Gd metallic foil of 2.5 mg/cm^2 thickness with a 7.0 mg/cm^2 Pb backing to stop the recoiling nuclei. In order to determine the optimum beam energy needed to produce ^{190}Tl and to identify the in-beam γ rays belonging to ^{190}Tl, relative γ-ray yields were measured at beam energies of 175 and 167 MeV. Inspecting the relative yields of the known γ lines previously assigned to ^{190}Tl [26] at different beam energies showed the optimum beam energy for producing ^{190}Tl to be 167 MeV, at which the γ-γ-t coincidence measurements were performed. Here, t refers to the relative time difference between any two coincident γ rays detected within $\pm$200 ns. A γ-ray detector array including 12 HPGe with BGO anti-Compton shields was used. In order to suppress the huge x-ray peaks of Gd and Pb, copper absorbers of 0.5 mm thickness were placed in front of the Ge detectors. The thick absorbers prohibited us from observing low-energy γ rays. The detectors were divided into three groups, of which the angle positions (and detector number at that angle) were 90° (3), $\pm$70° (6), and $\pm$45° (3) with respect to the beam direction, so that the DCO ratios (directional correlations of γ rays deexciting the oriented states) could be deduced from the coincidence data. All the detectors were calibrated with standard ^{133}Ba and ^{152}Eu sources; the typical energy resolution was 2.0–3.0 keV at full width at half-maximum for the 1332.5 keV line from ^{60}Co. The relative poor energy resolution was caused mainly by the neutron damage of Ge detectors. A total of about 125×10^6 γ-γ coincidence events were recorded in the experiment. After gain matching, these data were sorted into a $4k \times 4k$ symmetric $E_\gamma - E_\gamma$ matrix for off-line analysis.

To obtain the DCO ratios, a nonsymmetrized matrix with detectors at $\theta_2 = 90°$ against those at $\theta_1 = \pm 45°$ was constructed. The experimental DCO ratio was calculated by $R_{\mathrm{DCO}}(\gamma) = I_\gamma(\theta_1)/I_\gamma(\theta_2)$, where $I_\gamma(\theta_1)$ represents the intensities of an analyzed γ ray along the θ_1 axis in coincidence with the $M1$ transitions along θ_2 direction. Similarly, with the same gates on the θ_1 axis, coincidence spectra along the θ_2 axis were projected to determine $I_\gamma(\theta_2)$ [27]. In the present geometry, dipole transitions were adopted if $R_{\mathrm{DCO}}(\gamma)$ ratios were close to unity, and stretched quadrupole transitions were assumed if $R_{\mathrm{DCO}}(\gamma) \approx 0.7$. Additionally, in order to extract information concerning γ-ray anisotropies, the coincidence data were sorted into two asymmetric matrices whose x axis was the γ-ray energy deposited in the detectors at any angle and whose y axis was the γ-ray energy deposited in the detectors at $\pm$45° and 90°, respectively. By gating on the x axis with suitable γ rays, two spectra measured at $\pm$45° and 90° angle positions were obtained. After correcting for the overall detection efficiency of the detectors at each of the two angles and normalizing the two spectra with respect to each other, γ-ray anisotropy [$R_{\mathrm{ADO}}(\gamma)$] was deduced from the intensity ratio in the two spectra. Typical γ-ray anisotropies for the known γ rays observed in this experiment were 1.3 for stretched quadrupole transitions and 0.7 for stretched pure dipole transitions. Therefore we assigned the stretched quadrupole transition and stretched dipole transition to the γ rays of ^{190}Tl with anisotropies around 1.3 and 0.7, respectively.

Assignments of the observed γ rays to ^{190}Tl were based on the coincidences with the known γ rays with energies of 272.3, 280.5, and 382.4 keV [26]. The assignments were further confirmed by the measured relative γ-ray yields at different beam energies and Tl K x-ray coincident information. A gated spectrum was produced for each of the γ rays assigned to ^{190}Tl. Typical coincidence spectra are presented in Figs. 1 and 2, in which the main contamination comes from ^{191}Tl and ^{160}Gd. The 846.8-keV peak of ^{56}Fe is present in the spectra; this peak resulted from hitting the target chamber and beam line with the beam. Based on the analysis of the γ-γ coincidence relationships, a level scheme for ^{190}Tl is proposed and shown in Fig. 3. The order of transitions in the level scheme is fixed firmly with the help of interband transitions. In Fig. 3 the excitation energy of the β-decaying 7^+ isomer [28] was set to be zero as a reference because of its unknown excitation energy. As stated by Van Duppen *et al.* [23,24], unhindered α decay through the $Z = 82$ shell closure can identify intruder states in the daughter nuclei, and observation of unhindered α decay provided an ideal tool for identifying states with the same spin, parity, and configuration as the α-decaying parent state. The α-γ correlation measurements in the α decay of ^{194} Bi [23,24] established the spin and parity of $(\pi h_{9/2} \otimes \nu i_{13/2})_{10^-}$ for the state located 300 keV above the 7^+ isomer in ^{190}Tl. The 272.3 keV transition, corresponding well to the energy difference between the 572 keV level and the $(\pi h_{9/2} \otimes \nu i_{13/2})_{10^-}$ state as suggested in previous work [23,24], was observed the present work. Therefore, the excitation energies for the states observed in the present work were fixed with respect to the 7^+ isomer, and we adopt the spin and parity assignments for the low-lying states (as shown on the right-hand side of Fig. 3) [23,24]. Spins for the levels above the 300 keV $(\pi h_{9/2} \otimes \nu i_{13/2})_{10^-}$ state were proposed from the measured DCO and γ-ray anisotropy results. A weak 336.1 keV line is presented in Fig. 1(c), and its energy is exactly the sum of the 272.3 and 63.9 keV transitions [23,24]. But the 336.1 keV transition is too weak to confirm its coincidence relationship. We tentatively propose that the 336.1 keV transition depopulates the 11^- state. It

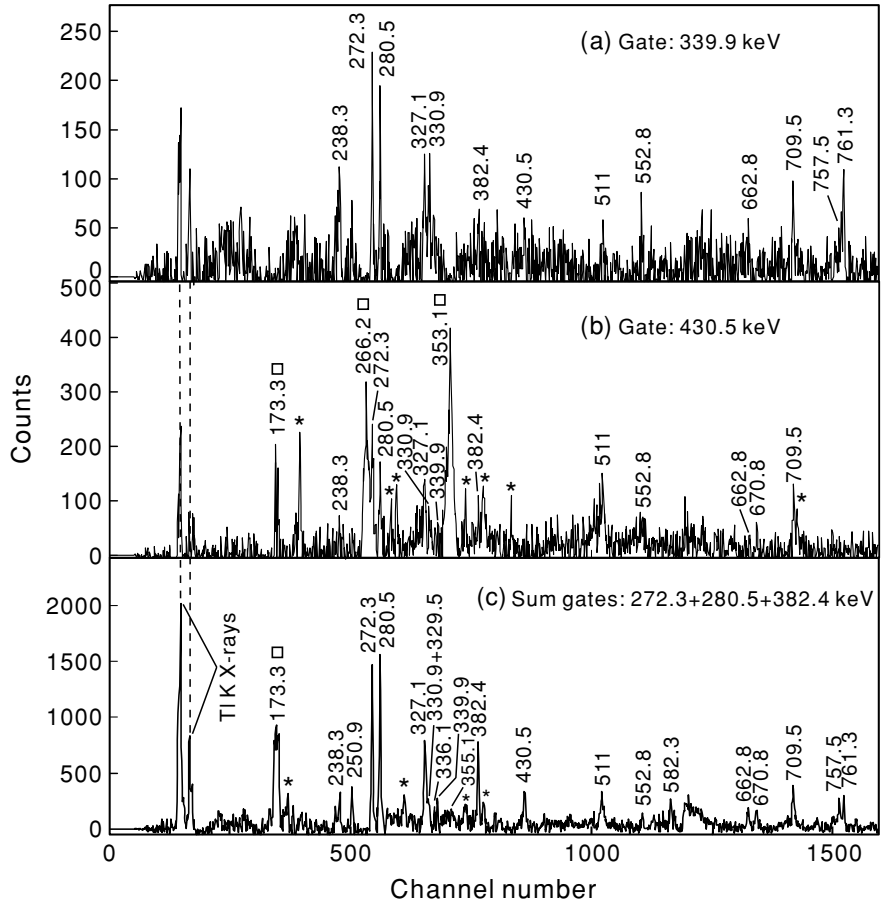

FIG. 1. The γ-ray spectra gated by the (a) 339.9 keV transition, (b) 430.5 keV transition, and (c) a sum coincidence spectrum from gates on the 272.3, 280.5, and 382.4 keV transitions. Asterisks indicate the contaminant γ rays from other fusion-evaporation products (mainly from ^{191}Tl). The lines marked with squares are from the ^{160}Gd target.

should be pointed out that the $(\pi h_{9/2} \otimes \nu i_{13/2})_{8^-}$ isomer reported by Kreiner *et al*. [26] was not confirmed in the α-γ correlation measurements, and the 9^- state was suggested to be the lowest member of the $(\pi h_{9/2} \otimes \nu i_{13/2})$ multiplet in ^{190}Tl [23,24].

For the $\Delta I = 1$ negative-parity rotational band shown in Fig. 3, the branching ratio, which is defined as

$$\lambda = \frac{T_\gamma(I \to I-2)}{T_\gamma(I \to I-1)}, \tag{1}$$

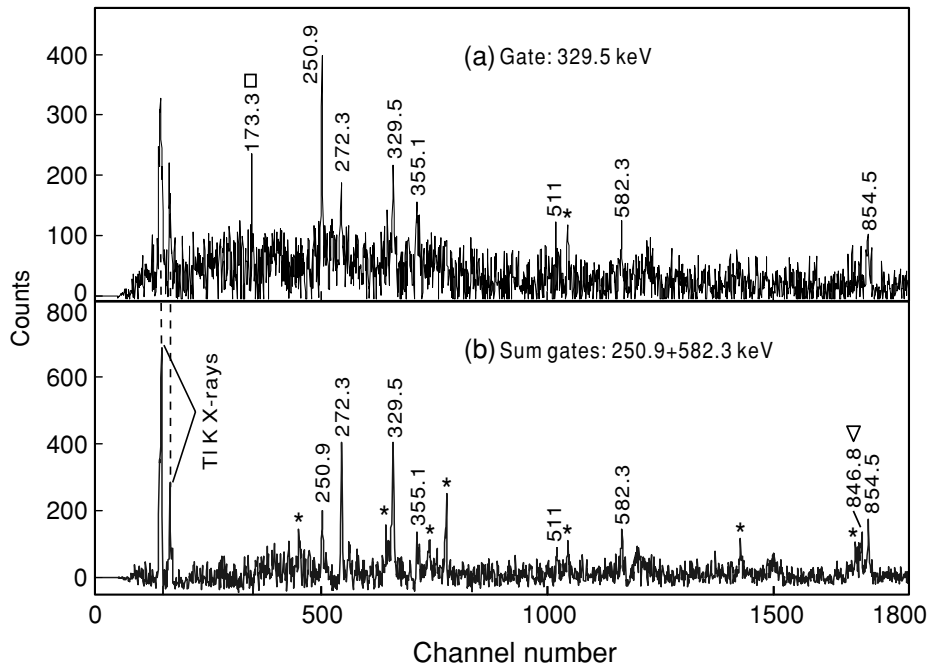

FIG. 2. (a) The γ-ray spectrum gated by the 329.5 keV transition. (b) A sum coincidence spectrum from gates on the 250.9 and 582.3 keV transitions. Asterisks indicate the contaminant γ rays (mainly from ^{191}Tl). The lines marked with a square and a triangle are from Coulomb excitation of ^{160}Gd (target) and ^{56}Fe (target chamber), respectively.

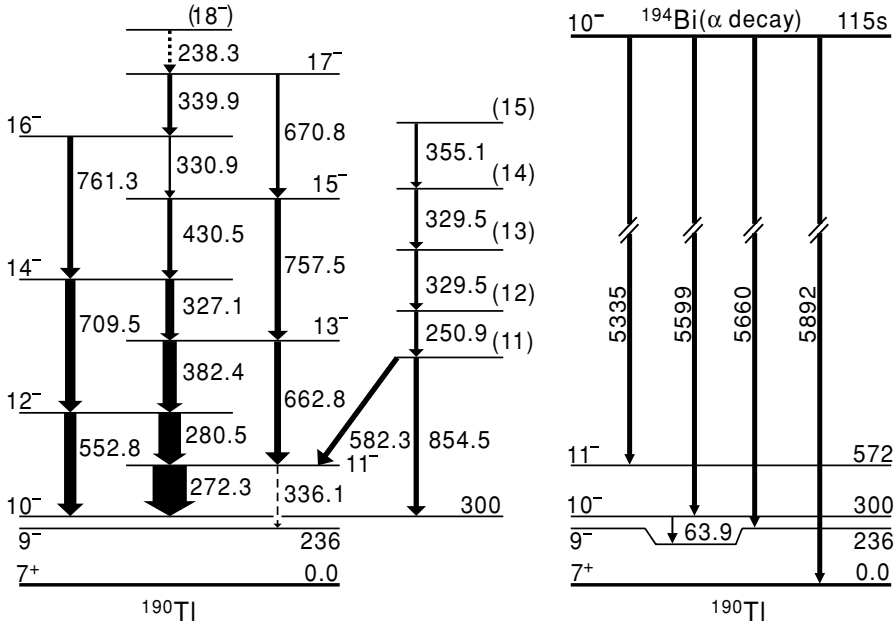

FIG. 3. Level scheme of ^{190}Tl deduced from (left) the present work and (right) α-decay scheme of ^{194}Bi [23,24]. The excitation energies are given relative to the 7^+ state. The widths of the arrows indicate the relative transition intensities in the level scheme of ^{190}Tl. Tentatively placed transitions are given by dashed arrows. Tentatively assigned spins are given in parentheses.

was extracted for most transitions. Here $T_\gamma(I \to I-2)$ and $T_\gamma(I \to I-1)$ are the γ-ray intensities of the $\Delta I = 2$ and 1 transitions, respectively. These intensities are measured in a summed coincidence spectrum gated by the transitions above the state of interest. The branching ratio was used to extract the reduced transition probability ratio, which is defined as [29]

$$\frac{B(M1; I \to I-1)}{B(E2; I \to I-2)} = 0.697 \frac{[E_\gamma(I \to I-2)]^5}{[E_\gamma(I \to I-1)]^3} \times \frac{1}{\lambda} \frac{1}{1+\delta^2} \left(\frac{\mu_N^2}{e^2 b^2} \right), \qquad (2)$$

where δ is the $E2/M1$ mixing ratio for the $\Delta I = 1$ transitions, and $E_\gamma(I \to I-1)$ and $E_\gamma(I \to I-2)$ are the $\Delta I = 1$ and 2 transition energies in units of mega electron volts, respectively. The mixing ratios $\delta \approx -0.4$ have been reported for the strongly coupled $\pi h_{9/2}$ bands in the neighboring odd-mass Tl isotopes [30] and for the oblate $\pi h_{9/2} \otimes \nu i_{13/2}$ band in ^{196}Tl [19]. Considering the similar band structure in these Tl isotopes, a constant value $\delta \approx -0.4$ was assumed in the present analysis; this value is quite consistent with the DCO and ADO ratios presented in Table I.

The relative intensities for some uncontaminated γ rays could be measured in the total projection spectrum. Most of the relative intensities were extracted from the spectra gated on the bottom transitions in the band. For some weak or heavily contaminated γ rays, only upper or lower limits are given based on their intensity balance. The relative intensities are corrected with the detection efficiencies. The γ-ray energies, spin, and parity assignments, relative γ-ray intensities, branching ratios λ, extracted $B(M1)/B(E2)$ values, DCO ratios, and anisotropies [$R_{\rm ADO}(\gamma)$] are collected in Table I.

III. DISCUSSION

A. Band properties in the rotating frame

The medium-mass Hg isotopes with $A \sim 190$, which are located in the transitional region between nuclei with large prolate deformation and spherical nuclei, are weakly oblate deformed and probably soft to γ deformation [31–33]. These Hg isotopes represent excellent cases where the cranked shell model (CSM) was successfully applied to oblate systems ($\gamma = -60^\circ$) rotating around an axis perpendicular to the symmetry axis [32,33]. In order to study the influence of rotation on the shape of the ^{190}Tl nucleus, and to compare the band properties between ^{190}Tl and its odd-A neighbors [32,34–36], it is necessary to transform the experimental excitation energies and spins into the rotating frame. The experimental Routhians and alignments have been extracted according to Ref. [37], and they are presented in Fig. 4. In such plots, the common Harris parameters $J_0 = 8.0\hbar^2$ MeV^{-1} and $J_1 = 40\hbar^4$ MeV^{-3} were used [38]. These parameters give nearly constant alignment for the first excited bands and zero alignment for the ground bands in the even-even Hg isotopes [31–33].

B. Theoretical calculations

In order to obtain a deeper understanding of the band properties in ^{190}Tl, we have performed cranked-shell-model (CSM) calculations by means of the total-Routhian-surface (TRS) method [39] in the three-dimensional deformation β_2, β_4, and γ space. The nonaxial deformed Woods-Saxon (WS) potential [40] was employed. Both monopole and quadrupole pairings [13,41] were included. To avoid the spurious pairing phase transition encountered in the BCS approach, we used the approximate particle number projection, named the Lipkin-Nogami pairing [42]. The pairing correlation is dependent

TABLE I. γ-ray transition energies, spin and parity assignments, γ-ray intensities, branching ratios, extracted $B(M1)/B(E2)$ ratios, DCO ratios, and γ-ray anisotropies in ^{190}Tl.

E_γ (keV)[a]	$J_i^\pi \rightarrow J_f^\pi$ [b]	I_γ [c]	λ [d]	$B(M1)/B(E2)$ [e]	R_{DCO}	R_{ADO}
272.3	$11^- \rightarrow 10^-$	100			0.99(12)	0.65(6)
336.1	$11^- \rightarrow 9^-$	$\leqslant$5.0	$\leqslant$0.06	$\geqslant$2.17		
280.5	$12^- \rightarrow 11^-$	66.1			1.02(12)	0.66(8)
552.8	$12^- \rightarrow 10^-$	32.2	0.52(3)	2.70(50)	0.7(28)	1.22(17)
382.4	$13^- \rightarrow 12^-$	41.5			1.01(15)	0.72(9)
662.8	$13^- \rightarrow 11^-$	20.1	0.56(6)	2.45(49)	0.69(20)	1.24(16)
327.1	$14^- \rightarrow 13^-$	26.1			1.04(15)	0.64(12)
709.5	$14^- \rightarrow 12^-$	30.5	1.32(9)	2.34(52)	0.70(20)	1.26(16)
430.5	$15^- \rightarrow 14^-$	14.7			0.99(22)	0.71(17)
757.5	$15^- \rightarrow 13^-$	18.6	1.26(14)	1.49(55)	0.70(21)	1.26(17)
330.9	$16^- \rightarrow 15^-$	6.8				0.66(18)
761.3	$16^- \rightarrow 14^-$	17.3	2.72(26)	1.56(62)	0.71(21)	1.24(17)
339.9	$17^- \rightarrow 16^-$	14.3				0.67(22)
670.8	$17^- \rightarrow 15^-$	10.7				1.22(19)
238.3	$(18^-) \rightarrow 17^-$	10.4				0.72(18)
250.9	$(12) \rightarrow (11)$	12.2				0.67(27)
329.5		$\leqslant$23.0[f]				0.65(26)
355.1	$(15) \rightarrow (14)$	8.8				0.63(26)
582.3	$(11) \rightarrow 11^-$	15.7				0.67(18)
854.5	$(11) \rightarrow 10^-$	15.4				0.70(18)

[a]Uncertainties between 0.1 and 0.5 keV.
[b]See text for details about the spin and parity assignments.
[c]Uncertainties between 5% and 30%. Normalized to the 272.3 keV transition.
[d]Branching ratio: $T_\gamma(I \rightarrow I-2)/T_\gamma(I \rightarrow I-1)$, $T_\gamma(I \rightarrow I-2)$, and $T_\gamma(I \rightarrow I-1)$ are the relative γ intensities of the $E2$ and $M1$ transitions depopulating level I, respectively.
[e]Extracted from the branching ratios, assuming $\delta = -0.4$.
[f]Unresolved doublet.

on rotational frequency ($\hbar\omega$) and deformation. In order to include such dependence in the TRS, we have done pairing-deformation-frequency self-consistent TRS calculations; i.e., for any given frequency and deformation, the pairing is self-consistently calculated by the HFB-like method [42]. At a given frequency, the deformation of a state is determined by minimizing the calculated TRS.

Figure 5 displays the calculated TRSs for the lowest configuration with $(\pi = -, \alpha = 1)$ at $\hbar\omega = 0.0, 0.1, 0.3, 0.4$ MeV. The calculations indicate a minimum in the total Routhian surface localized at a deformation ($\beta_2 \sim 0.17$) around the oblate collective axis ($\gamma = -60^\circ$). Although this minimum appears to be soft in the γ direction, it does not vary significantly with rotational frequency and remains near oblate for $\hbar\omega < 0.4$ MeV. With the calculated deformations, we plotted quasi-neutron Routhians as shown in Fig. 6. The calculations predict that a pair of $i_{13/2}$ neutron aligns at $\hbar\omega \approx 0.33$ MeV, while the $h_{11/2}$ proton alignment occurs at $\hbar\omega > 0.45$ MeV.

C. Configuration assignment

In this section an analysis of the γ-ray branching ratios is given for the band observed in ^{190}Tl. The $B(M1)/B(E2)$ ratios for a band based on multiquasiparticle excitation have been proved to be quite useful in characterizing the specific orbitals involved. Information concerning the configuration assignment for the band in ^{190}Tl can be obtained by comparing theoretical $B(M1)/B(E2)$ values with experimental ones. The experimental $B(M1)/B(E2)$ ratios have been deduced according to Eq. (2) described in the previous section and are plotted in Fig. 7. Theoretical $B(M1)$ values for a two-quasiparticle band in an odd-odd nucleus can be estimated by using the semiclassical formulas developed by Dönau and Frauendorf [43]:

$$B(M1; I \rightarrow I-1) = \frac{3}{8\pi}[(g_p - g_R)A + (g_n + g_R)B]^2\left(\mu_N^2\right), \tag{3}$$

$$A = \left(1 - \frac{K^2}{I^2}\right)^{1/2} \Omega_p - i_p \frac{K}{I}, \tag{4}$$

$$B = \left(1 - \frac{K^2}{I^2}\right)^{1/2} \Omega_n - i_n \frac{K}{I}. \tag{5}$$

Here $g_{p(n)}$, $i_{p(n)}$, and $\Omega_{p(n)}$ represent the g factor, the alignment, and the angular momentum component on the symmetry axis of the proton (neutron). These quantities can be extracted from the associated band properties in neighboring odd-A nuclei. It should be noted that the above equation is exact only for

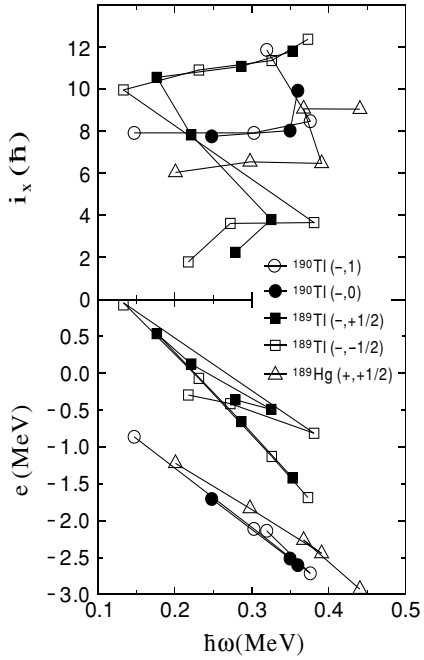

FIG. 4. Experimental alignments (top) and Routhians (bottom) as a function of the rotational frequency for the following structures: $\pi h_{9/2}$ coupled band of ^{189}Tl [35], $\nu i_{13/2}$ decoupled band of ^{189}Hg [31] and oblate rotational band of ^{190}Tl. The Harris reference parameters are chosen to be $J_0 = 8.0\hbar^2$ MeV^{-1} and $J_1 = 40\hbar^4$ MeV^{-3}.

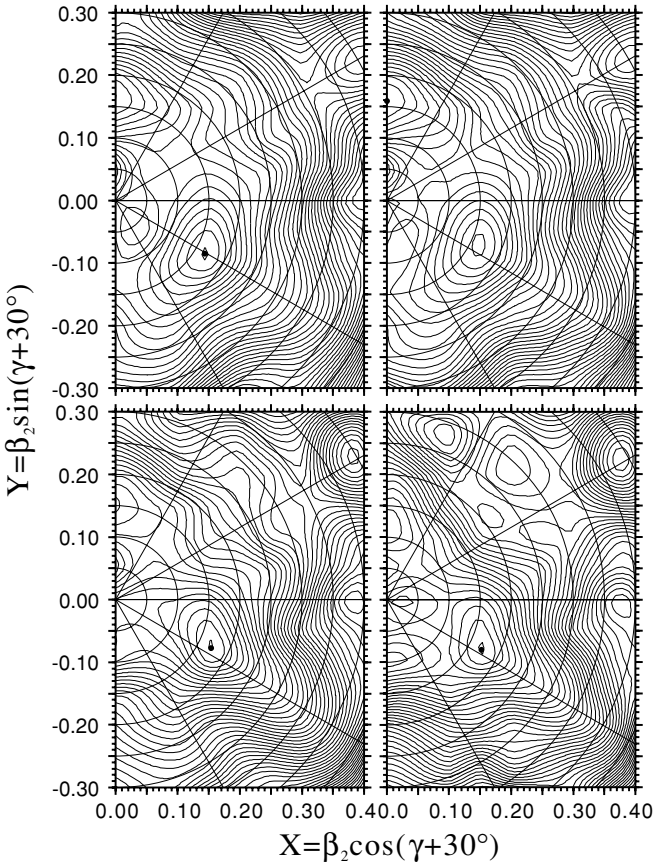

FIG. 5. Calculated total Routhian surfaces for the $(\pi, \alpha) = (-, 1)$ branch of the rotational band in ^{190}Tl. The upper left, upper right, lower left, and lower right panels correspond to $\hbar\omega = 0.0, 0.1, 0.3$, and 0.4 MeV. The energy difference between contours is 200 keV.

axially symmetric nuclear shapes, but it is certainly a good approximation for a small deviation of the nuclear shape from axial symmetry. The $B(E2)$ matrix element is expressed in the well-known geometrical manner [43]:

$$B(E2; I \rightarrow I-2) = \frac{5}{32\pi} Q_0^2 \cos^2(\gamma + 30^\circ) \times \left(1 - \frac{K}{I-1}\right)^2 (e^2 b^2). \quad (6)$$

This expression takes into account the effect of the sign of the triaxial deformation on $E2$ transition rate. The calculated $B(M1)/B(E2)$ ratios are compared with experimental ones in Fig. 7 under the assumption of an oblate $\pi h_{9/2} \otimes \nu i_{13/2}$ configuration ($\gamma = -60^\circ$) for the band in ^{190}Tl. In the calculations, the values $K = 5.0$, $i_p = 1.5$, and $i_n = 6.5$ were adopted from the $\pi h_{9/2}$ coupled band in ^{189}Tl [35,36] and $\nu i_{13/2}$ decoupled band in ^{189}Hg [32]. We used the measured g_p factor of 0.86 for the $(\pi h_{9/2})_{9/2^-}$ state in ^{189}Tl and g_n factor of –0.16 for the $(\nu i_{13/2})_{13/2^+}$ state in ^{189}Hg [44]. The rotational gyromagnetic factor was assumed to be $g_R = 0.3$, obtained from g-factor measurements of the 2^+ states in Os and Pt nuclei in the $A \sim 190$ mass region [44]. The quadrupole moment was set to $Q_0 = 3.75\ eb$, which corresponds approximately to the intrinsic quadrupole moment of the ground state in neighboring even-even nuclei [45]. The $\pi h_{9/2} \otimes \nu i_{13/2}$ band experiences a band crossing above a spin value of 15. The $i_{13/2}$ neutron alignment should result in an apparent increase of $B(M1)/B(E2)$ ratios as shown in Fig. 7. However, the last experimental point in Fig. 7 is just at the onset of the band crossing, and the completeness of the band crossing was not observed experimentally. In order to prove the $i_{13/2}$ neutron alignment, it is very important to extend the $\pi h_{9/2} \otimes \nu i_{13/2}$ band to higher spin values. The calculated $B(M1)/B(E2)$ curve corresponding to the $\pi i_{13/2} \otimes \nu i_{13/2}$ configuration significantly overestimates the experimental values as shown in Fig. 7. In this calculation, the values $K = 7.0$, $Q_0 = 6.7\ eb$, and $g_p = 1.22$ are used [36]. The above discussion favors the assignment of configuration $\pi h_{9/2} \otimes \nu i_{13/2}$ to the band observed in ^{190}Tl.

For oblate deformation in Tl nuclei with $Z = 81$ [34–36], the proton Nilsson orbitals originating from $\pi h_{9/2}$ spherical parentage are intruding from the above $Z = 82$ shell closure, and the Nilsson state with the largest projection on the nuclear symmetry axis ($\Omega_p = 9/2$) lies nearest to the proton Feimi surface, giving rise to strongly coupled bands in the odd-A Tl nuclei. On the other hand, for the odd-A Hg isotopes ranging from $A = 189$ to 199 [31–33], the neutron Fermi surface is near the top of the $\nu i_{13/2}$ subshell, and since the deformation is oblate the neutron angular momentum is approximately in a plane perpendicular to the symmetry axis, resulting in decoupled $\nu i_{13/2}$ bands in the odd-A Hg isotopes. From

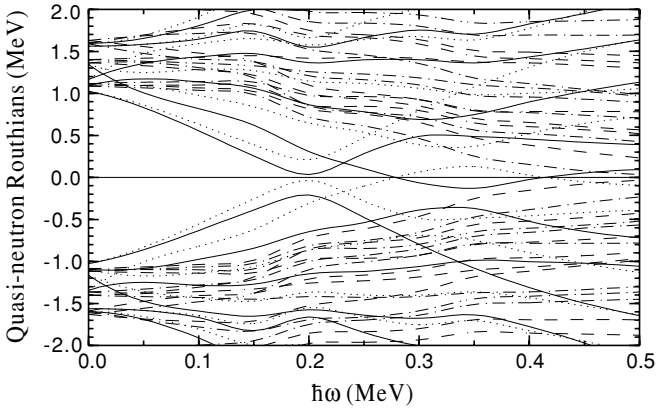

FIG. 6. Calculated quasi-neutron Routhians as a function of rotational frequency ($\hbar\omega$) in ^{190}Tl. The panel was calculated with $\beta_2 = 0.170$ ($\beta_4 = -0.010$) and $\gamma = -55.0^\circ$. The parity and signature (π, α) of the Routhians are represented as follows: (+, +1/2), solid curve; (+, −1/2), dotted curves; (−, +1/2), dash-dotted curves; and (−, −1/2), dashed curves. The lowest neutron Routhians with $\alpha = +1/2$ and $-1/2$ are the $i_{13/2}$ orbitals.

Fig. 4, we can see that the band in ^{190}Tl shows an initial alignment of about 8.0$\hbar$ at low rotational frequencies. Alignments are extracted to be about 2.0$\hbar$ and 6.0$\hbar$ at $\hbar\omega = 0.20$ MeV for the $\pi h_{9/2}$ band in ^{189}Tl and the $\nu i_{13/2}$ band in ^{189}Hg, respectively. According to the additivity rule in alignment [37,46], the initial alignment for the $\pi h_{9/2} \otimes \nu i_{13/2}$ band in ^{190}Tl is expected to be $i_x(pn) = i_x(\pi h_{9/2}) + i_x(\nu i_{13/2}) \approx 2.0 + 6.0 = 8.0\hbar$, which equals the experimentally extracted value for the band in ^{190}Tl. Figure 4 shows the onset of a backbending at $\hbar\omega \approx 0.35$ MeV for the band in ^{190}Tl. The CSM calculation predicts the neutron BC crossing at $\hbar\omega \approx 0.33$ MeV as shown in Fig. 6. The TRS calculation shown in Fig. 5 likely corresponds to the band observed in ^{190}Tl, as it comprises the yrast band. This configuration is γ soft at low rotational frequencies with a potential minimum at $\beta_2 \sim 0.17$ and $\gamma \sim -60^\circ$.

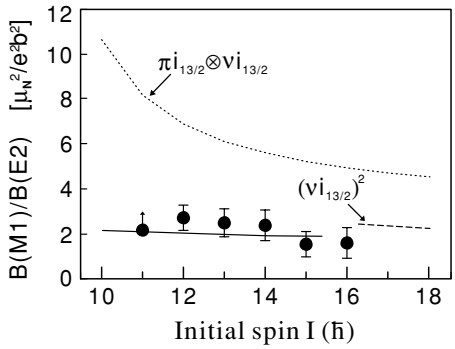

FIG. 7. Experimental $B(M1)/B(E2)$ ratios as a function of initial spin I for the $\pi h_{9/2} \otimes \nu i_{13/2}$ band, and theoretical prediction assuming $\gamma = -60^\circ$ as described in the text. The data point at spin 11 is a lower-limit value. Inclusion of the $\nu i_{13/2}$ alignment gives the dashed line. The dotted curve denotes the theoretical calculation for the $\pi i_{13/2} \otimes \nu i_{13/2}$ configuration.

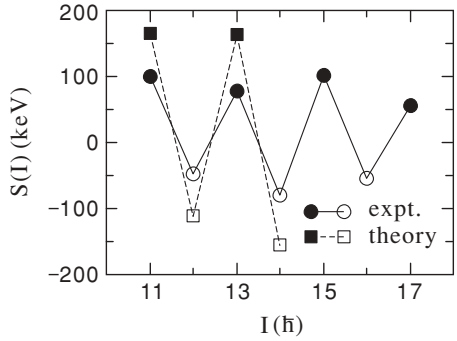

FIG. 8. Signature splitting $S(I)$ as a function of spin I for the $\pi h_{9/2} \otimes \nu i_{13/2}$ oblate band in ^{190}Tl. The circles represent experimental data, and the squares represent the calculated values. The filled and open symbols correspond to the favored and unfavored signatures, respectively.

D. Signature inversion

As described in the experimental section, spin and parity values were proposed for the $\pi h_{9/2} \otimes \nu i_{13/2}$ oblate band in ^{190}Tl on the basis of the complementary α-γ correlation measurements [23,24]. Although rotational bands based on the $\pi h_{9/2} \otimes \nu i_{13/2}$ oblate configuration were observed in doubly odd $^{192-200}$Tl nuclei [17–21], their spin assignments have remained uncertain because of experimental difficulties. An interesting phenomenon concerning the oblate band in ^{190}Tl is the distinctive energy staggering between the odd and even spin members (see Fig. 3), indicating an apparent energy signature splitting. With the configuration and spin-parity assignments in the present work, this staggering reveals that the signature splitting in the $\pi h_{9/2} \otimes \nu i_{13/2}$ band is inverted in the low spins; the expected $\alpha^f_{p-n} = \alpha^f_p + \alpha^f_n = 1/2 + 1/2 = 1$ favored signature branch (odd spin sequence) lies higher in energy than the $\alpha^{\rm uf}_{p-n} = \alpha^{\rm uf}_p + \alpha^f_n = 1/2 - 1/2 = 0$ unfavored signature branch (even spin sequence). Figure 8 presents plot of the signature splitting for the $\pi h_{9/2} \otimes \nu i_{13/2}$ oblate band in ^{190}Tl, defined as $S(I) = E(I) - [E(I+1) + E(I-1)]/2$. As shown in Fig. 8, the signature inversion in the low-spin regime is distinct. Since the oblate band experiences a band crossing above the state with spin value of 15$\hbar$, only the experimental data before the band crossing are presented in Fig. 8.

Due to the uncertainties of level spin assignments to the $\pi h_{9/2} \otimes \nu i_{13/2}$ bands in doubly odd $^{192-200}$Tl nuclei, Kreiner [22] has proposed two different models to interpret the level energy staggering. The first approach, utilizing a model based on two noninteracting quasiparticles plus a rotor, suggested that the level energy staggering is associated with the signature dependence of the Coriolis interaction [i.e., a $(-)^I$ effect, I being the total angular momentum]. The other model, which is almost identical to the first approach except for the inclusion of a residual proton-neutron (p-n) interaction, attributed the staggering to a J dependence of the p-n residual interaction ($\vec{J}$ being the total intrinsic angular momentum $\vec{J} = \vec{j}_p + \vec{j}_n$). These two models produced opposite phases of staggering [22]. This long-standing problem is now solved. In Fig. 8, the signature splitting calculated with the residual

pure proton-particle-neutron-hole interaction [22] is compared with the experimental observation. As shown in Fig. 8, it is the *p-n* residual interaction that reproduces the correct phase of the staggering at low spins observed in the $\pi h_{9/2} \otimes \nu i_{13/2}$ band of ^{190}Tl. If a strong repulsive matrix element of the *p-n* residual interaction acts in the maximally aligned intrinsic state $J = j_p + j_n = 11$, above the 10^- state a further alignment of the proton and neutron intrinsic spins is energetically more costly, and the system prefers to increase its total angular momentum at the expense of collective energy. As a consequence of this, the amplitude of the $J = 11$ component in the wave functions for the 11^- and higher states is drastically reduced, and at the same time the role of the $J = 10$ component becomes dominant [22]. This leads to energetically favored states with angular momenta of $I = R + J = R + 10 =$ even and unfavored states of $I - 1 = R + 10 - 1 =$ odd ($R =$ even is the collective angular momentum). Therefore signature inversion occurs at low spins for these bands.

As is well known, low-spin signature inversion in doubly odd nuclei was identified experimentally mainly by observing the change of the staggering phase at medium angular momentum [2,4–10]. For the $\pi h_{9/2} \otimes \nu i_{13/2}$ oblate configuration, the interplay between the Coriolis and *p-n* residual interactions, which favor the odd and even spins, respectively, is expected to produce at a given spin (inversion point) a mutual cancellation of the opposite contributions to the staggering. Above this inversion point, odd spins are favored energetically by the stronger Coriolis interaction, and thus the signature splitting reverts to the normal ordering. Because of the small kinematical moment of inertia associated with an oblate deformation, the Coriolis interaction in the $\pi h_{9/2} \otimes \nu i_{13/2}$ oblate configuration should be much stronger. Therefore we might expect to observe the inversion point in the $\pi h_{9/2} \otimes \nu i_{13/2}$ oblate band at lower spin value than in the prolate case. In order to prove this expectation, it is very desirable to extend the $\pi h_{9/2} \otimes \nu i_{13/2}$ oblate bands in odd-odd Tl nuclei to higher angular momenta.

Additionally, a side cascade, as shown in Fig. 3, was observed in ^{190}Tl. However, it is very difficult to associate the experimentally observed states with specific configurations owing to the lack of definite spin and parity assignments to these levels.

IV. SUMMARY AND CONCLUSIONS

The odd-odd nucleus ^{190}Tl has been produced in the bombardment of the ^{160}Gd target with ^{35}Cl projectiles. A rotational band has been established for ^{190}Tl. The $\pi h_{9/2} \otimes \nu i_{13/2}$ configuration with oblate deformation has been assigned to this band based on the measured in-band $B(M1)/B(E2)$ ratios and the existing knowledge of band structures in the neighboring nuclei. Spin and parity are proposed for the $\pi h_{9/2} \otimes \nu i_{13/2}$ oblate band by combining the present in-beam experimental results with the complementary α-γ correlation measurements in the α-decay studies of ^{194}Bi. With the configuration and spin-parity assignments, the $\pi h_{9/2} \otimes \nu i_{13/2}$ oblate band in ^{190}Tl displays low-spin signature inversion; the expected $\alpha^f_{p-n} = 1$ favored signature branch lies higher in energy than the $\alpha^{\rm uf}_{p-n} = 0$ unfavored signature branch. It is the first experimental observation of low-spin signature inversion for a band associated with the oblate $\pi h_{9/2} \otimes \nu i_{13/2}$ configuration. The two-quasiparticle-plus-rotor model, including a J-dependent *p-n* residual interaction, can interpret the low-spin signature inversion for the band built on the oblate $\pi h_{9/2} \otimes \nu i_{13/2}$ configuration.

ACKNOWLEDGMENTS

This work was supported by the National Natural Sciences Foundation of China (grants 10475097, 10375077, and 10221003) and the Major State Basic Research Development Program of China (contract G2000077402).

[1] A. Bohr and B. R. Mottelson, *Nuclear Structure* (W. A. Benjamin, Reading, Mass., 1975), Vol. 2.
[2] R. Bengtsson, H. Frisk, F. R. May, and J. A. Pinston, Nucl. Phys. **A415**, 189 (1984).
[3] I. Hamamoto, Nucl. Phys. **A520**, 297c (1990); Phys. Lett. **B235**, 221 (1990).
[4] Y. H. Zhang, M. Oshima, Y. Toh, X. H. Zhou, M. Koizumi, A. Osa, A. Kimura, Y. Hatsukawa, T. Morikawa, M. Nakamura, M. Sugawara, H. Kusakari, T. Komatsubara, K. Furuno, H. L. Wang, P. Luo, C. S. Wu, and F. R. Xu, Phys. Rev. C **68**, 054313 (2003).
[5] L. L. Riedinger, H. Q. Jin, W. Reviol, J.-Y. Zhang, R. A. Bark, G. B. Hagemann, and P. B. Semmes, Prog. Part. Nucl. Phys. **38**, 251 (1997).
[6] M. A. Cardona, A. J. Kreiner, D. Hojman, G. Levinton, M. E. Debray, M. Davidson, J. Davidson, R. Pirchio, H. Somacal, D. R. Napoli, D. Bazzacco, N. Blasi, R. Burch, D. De Acuña, S. M. Lenzi, G. Lo Bianco, J. Rico, and C. Rossi Alvarez, Phys. Rev. C **59**, 1298 (1999).
[7] R. A. Bark, J. M. Espino, W. Reviol, P. B. Semmes, H. Carlsson, I. G. Bearden, G. B. Hagemann, H. J. Jensen, I. Ragnarsson, L. L. Riedinger, H. Ryde, and P. O. Tjøm, Phys. Lett. **B406**, 193 (1997); **B416**, 453 (1998).
[8] Y. Liu, Y. Ma, H. Yang, and S. Zhou, Phys. Rev. C **52**, 2514 (1995).
[9] G. García Bermúdez and M. A. Cardona, Phys. Rev. C **64**, 034311 (2001).
[10] Y. H. Zhang, F. R. Xu, J. J. He, Z. Liu, X. H. Zhou, Z. G. Gan, T. Hayakawa, M. Oshima, T. Toh, T. Shizuma, J. Katakura, Y. Hatsukawa, M. Matsuda, H. Kusakari, M. Sugawara, K. Furuno, T. Komatsubara, T. Une, S. X. Wen, and Z. M. Wang, Eur. Phys. J. A **14**, 271 (2002).
[11] K. Hara and Y. Sun, Nucl. Phys. **A531**, 221 (1991).
[12] A. K. Jain and A. Goel, Phys. Lett. **B277**, 233 (1992).
[13] F. R. Xu, W. Satula, and R. Wyss, Nucl. Phys. **A669**, 119 (2000).
[14] C. Plettner, I. Ragnarsson, H. Schnare, R. Schwengner, L. Käubler, F. Dönau, A. Algora, G. de Angelis, D. R. Napoli, A. Gadea, J. Eberth, T. Steinhardt, O. Thelen, M. Hausmann,

A. Müller, A. Jungclaus, K. P. Lieb, D. G. Jenkins, R. Wadsworth, and A. N. Wilson, Phys. Rev. Lett. **85**, 2454 (2000).

[15] D. J. Hartley, A. Galindo-Uribarri, C. Baktash, M. P. Carpenter, M. Danchev, M. Devlin, C. J. Gross, R. V. F. Janssens, M. Lipoglavsek, E. Padilla, S. D. Paul, D. C. Radford, W. Reviol, L. L. Riedinger, D. G. Sarantites, D. Seweryniak, C.-H. Yu, and O. Zeidan, Phys. Rev. C **63**, 041301(R) (2001).

[16] D. Hojman, M. A. Cardona, D. R. Napoli, S. M. Lenzi, J. Davidson, M. Davidson, C. A. Ur, G. Lo Bianco, C. M. Petrache, M. Axiotis, D. Bazzacco, M. De Poli, G. de Angelis, E. Farnea, T. Kroell, S. Lunardi, N. Marginean, T. Martínez, R. Menegazzo, B. Quintana, and C. Rossi Alvarez, Phys. Rev. C **67**, 024308 (2003).

[17] A. J. Kreiner, A. Filevich, G. García Bermúdez, M. A. J. Mariscotti, C. Baktash, E. der Mateosian, and P. Thieberger, Phys. Rev. C **21**, 933 (1980).

[18] A. J. Kreiner, M. Fenzl, U. Heim, and W. Kutschera, Phys. Rev. C **20**, 2205 (1979).

[19] A. J. Kreiner, M. Fenzl, and W. Kutschera, Nucl. Phys. **A308**, 147 (1978).

[20] A. J. Kreiner, M. Fenzl, S. Lunardi, and M. A. J. Mariscotti, Nucl. Phys. **A282**, 243 (1977).

[21] A. J. Kreiner, M. A. J. Mariscotti, C. Baktash, E. der Mateosian, and P. Thieberger, Phys. Rev. C **23**, 748 (1981).

[22] A. J. Kreiner, Phys. Rev. C **22**, 2570 (1980).

[23] P. Van Duppen, P. Decrock, P. Dendooven, M. Huyse, G. Reusen, and J. Wauters, Nucl. Phys. **A529**, 268 (1991).

[24] M. Huyse, E. Coenen, K. Deneffe, P. Van Duppen, K. Heyde, and J. Van Maldegem, Phys. Lett. **B201**, 293 (1988).

[25] Y. A. Ellis-Akovali, K. S. Toth, C. R. Bingham, H. K. Carter, and D. C. Sousa, Phys. Rev. C **23**, 480 (1981).

[26] A. J. Kreiner, C. Baktash, G. García Bermúdez, and M. A. J. Mariscotti, Phys. Rev. Lett. **47**, 1709 (1981).

[27] A. Krämer-Flecken, T. Morek, R. M. Lieder, W. Gast, G. Hebbinghaus, H. M. Jäger, and W. Urban, Nucl. Instrum. Methods Phys. Res. A **275**, 333 (1989).

[28] R. Menges, U. Dinger, G. Huber, S. Schröder, S. Dutta, R. Kirchner, O. Klepper, T. Kühl, D. Marx, and G. Sprouse, G. S. I. Scientific Report 89-1, 33 (Gesellschaft für Sohwerionen forschung, Darmstac 1989).

[29] S. Juutinen, P. Ahonen, J. Hattula, R. Julin, A. Pakkanen, A. Virtanen, J. Simpson, R. Chapman, D. Clarke, F. Khazaie, J. Lisle, and J. N. Mo, Nucl. Phys. **A526**, 346 (1991).

[30] G. J. Lane, G. D. Dracoulis, A. P. Byrne, P. M. Walker, A. M. Baxter, J. A. Sheikh, and W. Nazarewicz, Nucl. Phys. **A586**, 316 (1995).

[31] F. Hannachi, G. Bastin, M. G. Porquet, C. Schück, J. P. Thibaud, C. Bourgeois, L. Hildingsson, D. Jerrestam, N. Perrin, H. Sergolle, F. A. Beck, T. Byrski, J. C. Merdinger, and J. Dudek, Nucl. Phys. **A481**, 135 (1988).

[32] I. G. Bearden, R. V. F. Janssens, M. P. Carpenter, E. F. Moore, I. Ahmad, P. J. Daly, R. Mayer, M. W. Drigert, P. B. Fernandez, B. Fornal, U. Garg, Z. W. Grabowski, T. L. Khoo, T. Lauritsen, W. Reviol, and D. Ye, Nucl. Phys. **A576**, 441 (1994).

[33] H. Hübel, A. P. Byrne, S. Ogaza, A. E. Stuchbery, G. D. Dracoulis, and M. Guttormsen, Nucl. Phys. **A453**, 316 (1986).

[34] A. J. Kreiner, J. Davidson, M. Davidson, H. Mosca, L. L. Riedinger, C. R. Bingham, M. W. Guidry, and A. C. Kahler, Phys. Rev. C **38**, 2674 (1988).

[35] M. G. Porquet, A. J. Kreiner, F. Hannachi, V. Vanin, G. Bastin, C. Bourgeois, J. Davidson, M. Debray, G. Falcone, A. Korichi, H. Mosca, N. Perrin, H. Sergolle, F. A. Beck, and J. C. Merdinger, Phys. Rev. C **44**, 2445 (1991).

[36] W. Reviol, L. L. Riedinger, J. M. Lewis, W. F. Mueller, C. R. Bingham, J. Y. Zhang, and B. E. Zimmerman, Phys. Scr. T **56**, 167 (1995).

[37] R. Bengtsson and S. Frauendorf, Nucl. Phys. **A327**, 139 (1979).

[38] M. Guttormsen, K. P. Blume, Y. K. Agarwal, A. V. Grumbkow, K. Hardt, H. Hübel, J. Recht, and P. Schüler, Z. Phys. A **312**, 155 (1983).

[39] W. Nazarewicz, R. Wyss, and A. Johnson, Phys. Lett. **B225**, 208 (1989).

[40] W. Nazarewicz, J. Dudek, R. Bengtsson, I. Ragnarsson, Nucl. Phys. **A435**, 397 (1985).

[41] W. Satula and R. Wyss, Phys. Rev. C **50**, 2888 (1994).

[42] W. Satula, R. Wyss, P. Magierski, Nucl. Phys. **A578**, 45 (1994).

[43] F. Dönau, Nucl. Phys. **A471**, 469 (1987); F. Dönau and S. Frauendorf, *Proceedings of the Conference on High Angular Momentum Properties of Nuclei, Oak Ridge, Tonn.,* edited by N. R. Johnson (Harwood Academic, Chur, Switzerland, 1982), p. 143.

[44] P. Raghavan, At. Data Nucl. Data Tables **42**, 189 (1989), and references therein.

[45] S. Raman, C. W. Nestor, Jr., and P. Tikkanen, At. Data Nucl. Data Tables **78**, 1 (2001), and references therein.

[46] R. Bengtsson and S. Frauendorf, Nucl. Phys. **A314**, 27 (1979).